Skyrmion versus vortex flux lattices in *p*-wave superconductors

Qi Li,[1,2] John Toner,[1] and D. Belitz[1,3]
[1]*Department of Physics and Institute of Theoretical Science, University of Oregon, Eugene, Oregon 97403, USA*
[2]*Department of Physics and Condensed Matter Theory Center, University of Maryland, College Park, Maryland 20742, USA*
[3]*Materials Science Institute, University of Oregon, Eugene, Oregon 97403, USA*
(Received 28 November 2007; revised manuscript received 21 November 2008; published 26 January 2009)

p-wave superconductors allow for topological defects known as skyrmions, in addition to the usual vortices that are possible in both *s*-wave and *p*-wave materials. In strongly type-II superconductors in a magnetic field, a skyrmion flux lattice yields a lower free energy than the Abrikosov flux lattice of vortices and should thus be realized in *p*-wave superconductors. We analytically calculate the energy per skyrmion, which agrees very well with numerical results. From this, we obtain the magnetic induction B as a function of the external magnetic field H and the elastic constants of the skyrmion lattice near the lower critical field H_{c1}. Together with the Lindemann criterion, these results suffice in predicting the melting curve of the skyrmion lattice. We find a striking difference in the melting curves of vortex and skyrmion lattices: while the former is separated at all temperatures from the Meissner phase by a vortex liquid phase, the skyrmion lattice phase shares a direct boundary with the Meissner phase. That is, skyrmion lattices *never* melt near H_{c1} while vortex lattices *always* melt sufficiently close to H_{c1}. This allows for a very simple test for the existence of a skyrmion lattice. Possible muon spin rotation experiments to detect skyrmion lattices are also discussed.

DOI: 10.1103/PhysRevB.79.014517 PACS number(s): 74.50.+r, 74.70.Pq, 74.25.Fy

I. INTRODUCTION

One of the most fascinating phenomena exhibited by conventional *s*-wave type-II superconductors is the appearance of an Abrikosov flux lattice of vortices in the presence of an external magnetic field $\boldsymbol{H}$ in a range $H_{c1}<|H|<H_{c2}$ between a lower critical field H_{c1} and an upper critical field H_{c2}.[1] It has been known for quite some time both theoretically[2–5] and experimentally[6,7] that these flux lattices can melt. The melting curve separates an Abrikosov vortex lattice phase from a vortex liquid phase, and the vortex lattice was found to melt in the vicinity of both H_{c1} and H_{c2}, as shown in Fig. 1. The melting occurs because the elastic constants of the flux lattice (i.e., the shear, bulk, and tilt moduli) vanish exponentially as a function of the growing lattice constant near these field values. As a result, in clean superconductors, root-mean-square positional thermal fluctuations $\sqrt{\langle|\boldsymbol{u}(\boldsymbol{x})|^2\rangle}$ grow exponentially as a function of the lattice constant when these fields are approached. According to the Lindemann criterion, when these fluctuations become comparable to the lattice constant a, the translational order of the flux lattice is destroyed, i.e., the lattice melts.

Vortices are topological defects in the texture of the superconducting order parameter, and in *s*-wave superconductors, where the order parameter is a complex scalar, only one type of defect is possible. In *p*-wave superconductors, the more complicated structure of the order parameter allows for an additional type of topological defect known as a skyrmion. In contrast to vortices, skyrmions do not involve a singularity at the core of the defect; rather, the order-parameter field is smooth everywhere, as illustrated in Fig. 2.

Skyrmions were first introduced in a nuclear physics context by Skyrme,[8] and slight variations in this concept[9] were later shown or proposed to be important in superfluid ^{3}He,[10,11] in the blue phases of liquid crystals,[12] in quantum Hall systems,[13,14] in itinerant ferromagnets,[15] and in *p*-wave superconductors.[16] In the latter case, skyrmions carry a quantized magnetic flux, as do vortices, although the lowest energy skyrmion contains two flux quanta while the lowest energy vortex contains just one. For strongly type-II superconductors, skyrmions have a lower free energy than vortices, and a vortex lattice should thus be the state that occurs naturally.[16]

Recent evidence of *p*-wave superconductivity in Sr_2RuO_4 (Refs. 17–19) provides motivation for further exploration of the properties of skyrmion flux lattices in such systems.[20] It

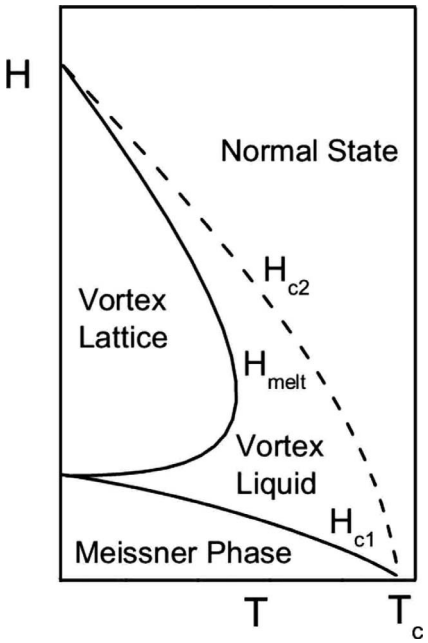

FIG. 1. External field (H) vs temperature (T) phase diagram for vortex flux lattices. Shown are the Meissner phase, the vortex lattice phase, the vortex liquid, and the normal state. Notice that the vortex lattice is never stable sufficiently close to H_{c1}.

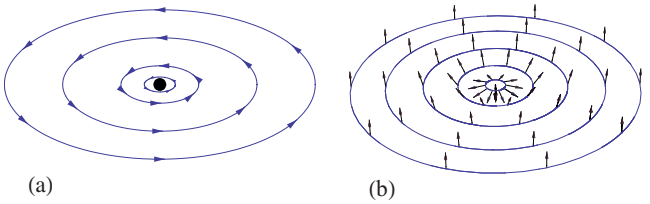

FIG. 2. (Color online) Order parameter configurations showing (a) a vortex and (b) a skyrmion. The local order parameters are represented by arrows on loci of equal distance from the center of the defect. If the order-parameter space is two dimensional, only vortices are possible, and there is a singularity at the center of each vortex, (a). If the order-parameter space is three dimensional, a skyrmion can form instead, where the spin direction changes smoothly from "down" at the center to "up" at infinity, (b).

was shown numerically by Knigavko *et al.*[16] that the interaction between skyrmions falls off only as $1/R$ with distance R, as opposed to the exponentially decaying interaction between vortices. As a result, skyrmion lattices have a very different dependence of the magnetic induction on the external magnetic field near H_{c1} than do vortex lattices. In this paper we confirm and expand on these results. We show analytically that the skyrmion-skyrmion interaction, in addition to a leading $1/R$ dependence, has a correction proportional to $\ln R/R^2$ that explains a small discrepancy between the numerical results in Ref. 16 and a strict $1/R$ fit; moreover we calculate the interaction energy up to $O(1/R^2)$. We further show that the melting curve of a skyrmion lattice is qualitatively different from that of a vortex lattice. Namely, skyrmion lattices melt *nowhere* in the vicinity of H_{c1} so there is a direct transition from the Meissner phase to the skyrmion lattice (see Fig. 8 below). Finally, we predict and discuss the magnetic induction distribution $n(B)$ of a skyrmion lattice state as observed in a muon spin rotation (μSR) experiment. For a vortex lattice, the exponential decay of the magnetic induction B at large distances from a vortex core implies $n(B) \propto \ln B/B$. For a skyrmion lattice, we find that B decays only algebraically, which leads to $n(B) \propto B^{-3/2}$. Some of these results have been reported before in Ref. 21.

The paper is organized as follows. In Sec. II we review the formulation in Ref. 16 of the skyrmion problem. In particular, we start from the Ginzburg-Landau (GL) model for p-wave superconductors and consider the free energy in a London approximation. We parametrize the skyrmion solution of the saddle-point equations and express the energy in terms of the solution of the saddle-point equations. In Sec. III we analytically solve these saddle-point equations perturbatively for large skyrmion radius R, and we calculate the energy of a single skyrmion as a power series in $1/R$ to order $1/R^2$. In Sec. IV we determine the elastic properties of the skyrmion lattice, and we predict the magnetic induction distribution $n(B)$ as observed in a μSR experiment.

II. FORMULATION OF THE SKYRMION PROBLEM

In this section we review the formulation of the skyrmion problem presented in Ref. 16, which derived an effective action that allows for skyrmions as saddle-point solutions. The resulting ordinary differential equations (ODEs) describing skyrmions[16] are the starting point for our analytic treatment.

A. Action in the London approximation

We start from a Landau-Ginzburg-Wilson (LGW) functional appropriate for describing spin-triplet superconducting order,

$$S = \int d\boldsymbol{x}\, \mathcal{L}(\boldsymbol{\psi}(\boldsymbol{x}), \boldsymbol{A}(\boldsymbol{x})), \tag{2.1a}$$

with an action density

$$\mathcal{L}(\boldsymbol{\psi}, \boldsymbol{A}) = t|\boldsymbol{\psi}|^2 + u|\boldsymbol{\psi}|^4 + v|\boldsymbol{\psi} \times \boldsymbol{\psi}^*|^2 + \frac{1}{2m}|\boldsymbol{D}\psi|^2 + \frac{1}{8\pi}(\boldsymbol{\nabla} \times \boldsymbol{A})^2. \tag{2.1b}$$

Here $\boldsymbol{\psi}(\boldsymbol{x})$ is a three-component complex order-parameter field,[22] $\boldsymbol{A}(\boldsymbol{x})$ is the electromagnetic vector potential, and $\boldsymbol{D} = \boldsymbol{\nabla} - iq\boldsymbol{A}$ denotes the gauge-invariant gradient operator. m and q are the mass and the charge, respectively, of a Cooper pair, and we use units such that $\hbar = c = 1$. t, u, and v are the parameters of the LGW theory.

Let us look for saddle-point solutions to this action. In a large part of parameter space, namely, for $v < 0$ and $u > -v$, the stable saddle-point solution has the form $\boldsymbol{\psi}(\boldsymbol{x}) \equiv \boldsymbol{\psi} = f_0(1, i, 0)/\sqrt{2}$, where the amplitude f_0 is determined by minimization of the free energy.[23] This is known as the β phase, and it is considered the most likely case to be realized in any of the candidates for p-wave superconductivity.[24] Fluctuations about this saddle point are conveniently parametrized by writing the order-parameter field as

$$\boldsymbol{\psi}(\boldsymbol{x}) = \frac{1}{\sqrt{2}} f(\boldsymbol{x})[\hat{\boldsymbol{n}}(\boldsymbol{x}) + i\hat{\boldsymbol{m}}(\boldsymbol{x})], \tag{2.2}$$

where $\hat{\boldsymbol{n}}(\boldsymbol{x})$ and $\hat{\boldsymbol{m}}(\boldsymbol{x})$ are unit real orthogonal vectors in order-parameter space and $f(\boldsymbol{x})$ is the modulus of order parameter. With this parametrization, the action density can be written

$$\mathcal{L} = tf^2 + (u+v)f^4 + \frac{1}{2m}\left\{(\boldsymbol{\nabla} f)^2 + f^2\left[\frac{1}{2}(\partial_i \hat{\boldsymbol{l}})^2 + (\hat{\boldsymbol{n}} \cdot \partial_i \hat{\boldsymbol{m}} - qA_i)^2\right]\right\} + \frac{1}{8\pi}(\boldsymbol{\nabla} \times \boldsymbol{A})^2, \tag{2.3}$$

where $\hat{\boldsymbol{l}} = \hat{\boldsymbol{n}} \times \hat{\boldsymbol{m}}$, summation over repeated indices is implied, and we have made use of the identities listed in Appendix A.

There are two length scales associated with the action density [Eq. (2.3)]. The coherence length ξ is determined by comparing the f^2 term with the $(\boldsymbol{\nabla} f)^2$ term,

$$\xi = 1/\sqrt{2m|t|}. \tag{2.4a}$$

It is the length scale over which the amplitude of the order parameter will typically vary. The London penetration depth λ is determined by comparing the $\boldsymbol{A}^2$ term with the $(\boldsymbol{\nabla} \times \boldsymbol{A})^2$ term,

$$\lambda = \sqrt{m/4\pi q^2 \langle f \rangle^2}. \tag{2.4b}$$

The ratio of these two length scales, $\kappa \equiv \lambda/\xi$, is the Ginzburg-Landau parameter. Now we write $f(\boldsymbol{x}) = f_0 + \delta f(\boldsymbol{x})$, with $f_0 = \sqrt{-t/2(u+v)}$. Deep inside the superconducting phase, where $-t > 0$ is large, the amplitude fluctuations δf are massive. Moreover to study low-energy excitations, one can integrate out f in a tree approximation. This approximation becomes exact in the limit of large κ and is known in this context as the London approximation. We introduce dimensionless quantities by measuring distances in units of λ and the action in units of $\Phi_0^2/32\pi^3\lambda$, and we introduce a dimensionless vector potential $\boldsymbol{a} = 2\pi\lambda \boldsymbol{A}/\Phi_0$, with $\Phi_0 = 2\pi/q$ as the magnetic-flux quantum. Ignoring constant contributions to the action, we can then write the action density in London approximation as follows:[16]

$$\mathcal{L}_L = \frac{1}{2}(\partial_i \hat{\boldsymbol{l}})^2 + (\hat{\boldsymbol{n}} \partial_i \hat{\boldsymbol{m}} - a_i)^2 + \boldsymbol{b}^2, \tag{2.5}$$

with $\boldsymbol{b} = \boldsymbol{\nabla} \times \boldsymbol{a}$. The above derivation makes it clear that this effective action is a generalization of the $O(3)$ nonlinear sigma model [represented by the first term on the right-hand side of Eq. (2.5)] that one obtains for a real three-vector order parameter by integrating out the amplitude fluctuations in tree approximation.[25]

B. Saddle-point solutions of the effective action

We now are looking for saddle-point solutions to the effective-field theory [Eq. (2.5)]. Considering $\hat{\boldsymbol{l}}$ and $\hat{\boldsymbol{n}}$ as independent variables, and minimizing with respect to $\hat{\boldsymbol{l}}$ subject to the constraints $\hat{\boldsymbol{l}}^2 = \hat{\boldsymbol{n}}^2 = 1$ and $\hat{\boldsymbol{l}} \cdot \hat{\boldsymbol{n}} = 0$, yields

$$\boldsymbol{\nabla}^2 \hat{\boldsymbol{l}} - \hat{\boldsymbol{l}}(\hat{\boldsymbol{l}} \cdot \boldsymbol{\nabla}^2 \hat{\boldsymbol{l}}) + 2J_i(\hat{\boldsymbol{l}} \times \partial_i \hat{\boldsymbol{l}}) = 0, \tag{2.6a}$$

with

$$\boldsymbol{J} = \boldsymbol{\nabla} \times \boldsymbol{b} \tag{2.6b}$$

as the supercurrent. The variation with respect to $\boldsymbol{a}$ is straightforward and yields a generalized London equation,

$$a_i + J_i = \hat{\boldsymbol{n}} \partial_i \hat{\boldsymbol{m}}. \tag{2.6c}$$

It is convenient to take the curl of Eq. (2.6c) and use Eq. (A3) to express the right-hand side of the resulting equation in terms of $\hat{\boldsymbol{l}}$. We then obtain the saddle-point equations as a set of coupled partial differential equations (PDEs) in terms of $\boldsymbol{b}$ and $\hat{\boldsymbol{l}}$ only:

$$b_i - \boldsymbol{\nabla}^2 b_i = \frac{1}{2}\epsilon_{ijk} \hat{\boldsymbol{l}} \cdot (\partial_j \hat{\boldsymbol{l}} \times \partial_k \hat{\boldsymbol{l}}), \tag{2.7a}$$

$$\boldsymbol{\nabla}^2 \hat{\boldsymbol{l}} - \hat{\boldsymbol{l}}(\hat{\boldsymbol{l}} \cdot \boldsymbol{\nabla}^2 \hat{\boldsymbol{l}}) + 2\epsilon_{ijk} \partial_j b_k (\hat{\boldsymbol{l}} \times \partial_i \hat{\boldsymbol{l}}) = 0. \tag{2.7b}$$

Notice that the right-hand side of Eq. (2.7a) is valid in this form only at points where $\hat{\boldsymbol{l}}(\boldsymbol{x})$ is differentiable [see Eq. (A3)]. Field configurations that obey these PDEs have an energy

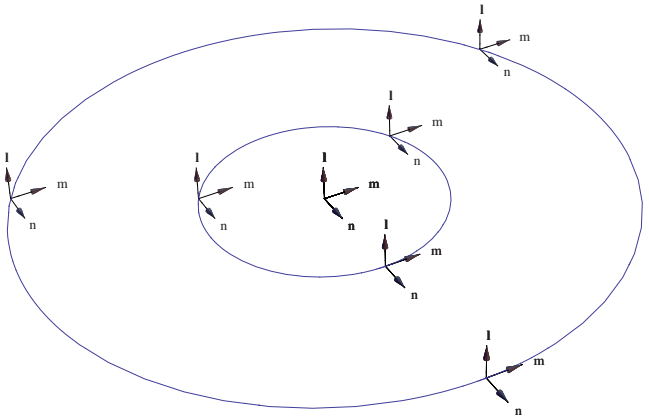

FIG. 3. (Color online) Configurations of the vectors $\hat{\ell}$, $\hat{m}$, and $\hat{n}$ in a Meissner phase. All three vectors point in the same direction everywhere.

$$E = \int d\boldsymbol{x} \left[\frac{1}{2}(\partial_i \hat{\boldsymbol{l}})^2 + (\hat{\boldsymbol{n}} \cdot \partial_i \hat{\boldsymbol{m}} - \boldsymbol{a})^2 + \boldsymbol{b}^2 - 2\boldsymbol{h} \cdot \boldsymbol{b} \right], \tag{2.8}$$

where we have added a uniform external magnetic field $\boldsymbol{h}$ measured in units of $\Phi_0/2\pi\lambda^2$. Notice that the energy depends on $\hat{\boldsymbol{n}}$ and $\hat{\boldsymbol{m}}$, whereas Eq. (2.7) depends only on $\hat{\boldsymbol{l}}$, and that different choices of $\hat{\boldsymbol{n}}$ and $\hat{\boldsymbol{m}}$ can lead to the same $\hat{\boldsymbol{l}}$. Therefore, a field configuration satisfying Eq. (2.7) is only necessary for making the energy stationary but not sufficient.

1. Meissner solution

A very simple order-parameter configuration consists of constant $\hat{\boldsymbol{n}}(\boldsymbol{x})$ and $\hat{\boldsymbol{m}}(\boldsymbol{x})$ everywhere (see Fig. 3). This leads to an $\hat{\boldsymbol{l}}(\boldsymbol{x}) \equiv \hat{\boldsymbol{l}}$ that is constant everywhere. Equation (2.7b) is then trivially satisfied. The right-hand side of Eq. (2.7a) vanishes, and hence the PDE for $\boldsymbol{b}$ reduces to the usual London equation with a solution $\boldsymbol{b}(\boldsymbol{x}) \equiv 0$ in the bulk. This solution describes a Meissner phase with energy $E_M = 0$.

2. Vortex solution

Now consider a field configuration where $\hat{\boldsymbol{n}}(\boldsymbol{x})$ and $\hat{\boldsymbol{m}}(\boldsymbol{x})$ are confined to a plane (say, the x-y plane) but rotate about an arbitrarily chosen point of origin,

$$\hat{\boldsymbol{n}}(\boldsymbol{x}) = (\cos\phi, \sin\phi, 0),$$

$$\hat{\boldsymbol{m}}(\boldsymbol{x}) = (-\sin\phi, \cos\phi, 0), \tag{2.9}$$

where ϕ denotes the azimuthal angle in the x-y plane with respect to the x axis. This field configuration, known as a vortex and shown in Fig. 4, corresponds to a constant $\hat{\boldsymbol{l}}$ everywhere except at the origin, where there is a singularity.

Therefore, the right-hand side of Eq. (2.7a) is not applicable, and we return to Eq. (2.6c), which takes the form

$$a_i + \epsilon_{ijk} \partial_j a_k = \partial_i \phi. \tag{2.10}$$

For any closed path $\mathcal{C}$ in the x-y plane that surrounds the origin, one has

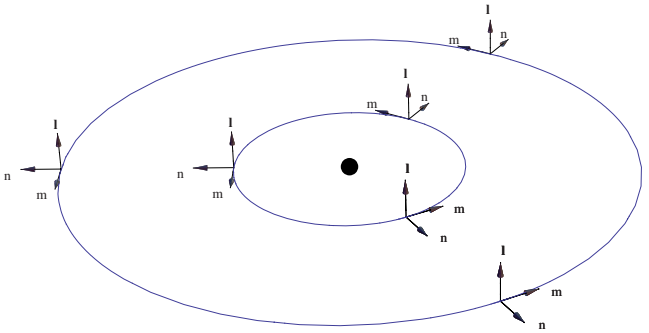

FIG. 4. (Color online) Configurations of the vectors $\hat{\ell}$, $\hat{m}$, and $\hat{n}$ for a vortex. $\hat{\ell}$ is constant, whereas $\hat{m}$ and $\hat{n}$ rotate about the vortex core. Notice that the vector shown in Fig. 2(a) is $\hat{n}$.

$$\oint_{\mathcal{C}} d\ell \cdot \nabla \phi(\boldsymbol{x}) = 2\pi, \tag{2.11a}$$

or, by Stokes' theorem,

$$\int_{\mathcal{A}} d\boldsymbol{s} \cdot [\nabla \times \nabla \phi(\boldsymbol{x})] = 2\pi, \tag{2.11b}$$

where $\mathcal{A}$ is the surface whose boundary is $\mathcal{C}$.[26] This quantization condition shows that, instead of Eq. (2.7a), we have

$$\boldsymbol{b}(\boldsymbol{x}) - \nabla^2 \boldsymbol{b}(\boldsymbol{x}) = 2\pi \hat{z} \delta(x) \delta(y). \tag{2.12}$$

This is solved by a $\boldsymbol{b}$ that is equal to the boundary-condition value everywhere along the z axis and that falls off exponentially away from the z axis. This solution is known as a vortex, and the amount of magnetic flux contained in one vortex is one flux quantum Φ_0.[26] It is the precise analog of, and indeed essentially identical to, the familiar vortex in conventional s-wave superconductors.

The energy of a vortex given by Eq. (2.12), as calculated from Eq. (2.8), is logarithmically infinite. This is due to the pointlike nature of the vortex core where the amplitude of the order parameter goes discontinuously to zero. In reality, the amplitude cannot vary on length scales shorter than the coherence length ξ, which provides an ultraviolet cutoff. The energy is then proportional to $\ln \kappa$.[1] In an external magnetic field this energy cost is offset by the magnetic energy gain due to letting some flux penetrate the sample. For κ larger than a critical value $\kappa_c = 1/\sqrt{2}$, and for external fields larger than the lower critical field H_{c1}, a hexagonal lattice of vortices has a lower energy than the Meissner phase. This state is known as an Abrikosov flux lattice and is precisely the same as that in conventional s-wave superconductors.[1]

3. Skyrmion solution

Due to the three-component nature of the order parameter, more complicated solutions of the saddle-point equations can be constructed for which the vector $\hat{\boldsymbol{l}}$ is not fixed. Let θ be the angle between $\hat{\boldsymbol{l}}$ and the z axis, and consider a cylindrically symmetric field configuration parametrized as

$$\hat{\boldsymbol{l}} = \hat{\boldsymbol{e}}_z \cos\theta(r) + \hat{\boldsymbol{e}}_r \sin\theta(r),$$

$$\hat{\boldsymbol{n}} = [\hat{\boldsymbol{e}}_z \sin\theta(r) - \hat{\boldsymbol{e}}_r \cos\theta(r)]\sin\varphi + \hat{\boldsymbol{e}}_\varphi \cos\varphi,$$

$$\hat{\boldsymbol{m}} = [\hat{\boldsymbol{e}}_z \sin\theta(r) - \hat{\boldsymbol{e}}_r \cos\theta(r)]\cos\varphi - \hat{\boldsymbol{e}}_\varphi \sin\varphi. \tag{2.13}$$

For this to minimize the energy, $\hat{\boldsymbol{l}}$ at large distances from the origin must be constant because of the first term in the energy [Eq. (2.8)]. Moreover for a skyrmion centered in a cylinder of radius R, we take $\hat{\boldsymbol{l}}$ to point in the $+z$ direction for $r=R$, $\theta(r=R)=0$. The quantization condition analogous to Eq. (2.11b) for the vortex is[27,28]

$$\int dxdy \epsilon_{ij} \hat{\boldsymbol{l}} \cdot (\partial_i \hat{\boldsymbol{l}} \times \partial_j \hat{\boldsymbol{l}}) = 8\pi. \tag{2.14}$$

To be consistent with this, $\hat{\boldsymbol{l}}$ must point in the $-z$ direction at the origin, $\theta(r=0)=\pi$.

Equation (2.13) parametrizes the order parameter in terms of a function $\theta(r)$. In addition, the energy depends on the vector potential which we take to be purely azimuthal, in accordance with our cylindrically symmetric ansatz,

$$\boldsymbol{a}(\boldsymbol{x}) = a(r)\hat{\boldsymbol{e}}_\varphi. \tag{2.15}$$

With this parametrization, we obtain from Eq. (2.8) the energy per unit length, along the cylinder axis, of a cylindrically symmetric skyrmion in a region of radius R,

$$E/E_0 = \frac{1}{2}\int_0^R dr r \left\{ [\theta'(r)]^2 + \frac{1}{r^2}\sin^2\theta(r) \right\} + \int_0^R dr r \left\{ \frac{1}{r}[1+\cos\theta(r)] + a(r) \right\}^2 + \int_0^R dr r \left[\frac{a(r)}{r} + a'(r) \right]^2, \tag{2.16}$$

where $E_0 = (\Phi_0/4\pi\lambda)^2$. This expression was first obtained in Ref. 16. The three terms correspond to the three terms in the London action [Eq. (2.5)]. They represent the energy of the nonlinear sigma model, the kinetic energy of the supercurrent, and the magnetic energy, respectively. Minimization of E with respect to $\theta(r)$ and $a(r)$ yields Euler-Lagrange equations,

$$\theta''(r) + \frac{1}{r}\theta'(r) = \frac{-\sin\theta(r)}{r}\left[\frac{2+\cos\theta(r)}{r} + 2a(r) \right], \tag{2.17a}$$

$$a''(r) + \frac{1}{r}a'(r) - \frac{1}{r^2}a(r) = a(r) + \frac{1}{r}[1+\cos\theta(r)]. \tag{2.17b}$$

This set of coupled nonlinear ODEs must be solved subject to the boundary conditions $\theta(r=0)=\pi$ and $\theta(r=R)=0$, as explained above. The solution is known as a skyrmion, and each skyrmion contains two flux quanta.[28] Since Eq. (2.7) are necessary for making the energy stationary, the solution of Eq. (2.17), inserted in Eqs. (2.13) and (2.15), is guaranteed to be a solution of Eq. (2.7) as well.

The energy of a single skyrmion is finite even in London approximation (see Sec. III below). For large values of the Ginzburg-Landau parameter κ, a skyrmion therefore has a lower energy than a vortex, and the value of the lower critical field H_{c1}, at which the Meissner phase becomes unstable, is correspondingly lower for skyrmions than for vortices. This is the basis for the expectation that, in strongly type-II (i.e., large-κ) *p*-wave superconductors, a skyrmion flux lattice will be realized rather than a vortex flux lattice.

III. ANALYTIC SOLUTION OF THE SINGLE-SKYRMION PROBLEM

We now need to solve the coupled ODEs [Eq. (2.17)]. Due to their nonlinear nature, this is a difficult task, and in Ref. 16 it was done numerically. It, however, turns out that one can construct a perturbative analytical solution in the limit of large skyrmion radius, $R \gg \lambda$, with λ/R as a small parameter. This provides information about the superconducting state near H_{c1}, where the system is always in that limit. We will construct the perturbative solution, and calculate the energy, to second order in the small parameter. Our general strategy is as follows. We use Eq. (2.17b) to iteratively express a in terms of θ and its derivatives. Substitution in Eq. (2.17a) then yields a closed ODE for $\theta(r)$ that has to be solved.

A. Zeroth order solution

Let us first consider $R=\infty$. For $r \to \infty$, the left-hand side of Eq. (2.17b) falls off as $1/r^2$, and hence the vector potential, to zeroth order for large r, is given by

$$a_\infty(r) = -\frac{1}{r}[1+\cos\,\theta(r)]. \tag{3.1}$$

Note that we use the *exact* $\theta(r)$ in this expression, *not* the zeroth order approximation to it. Since we can only compute $\theta(r)$ perturbatively, this expression for the zeroth order vector potential will itself have to be expanded perturbatively later. Substitution in Eq. (2.17a) yields

$$r^2\theta''(r) + r\theta'(r) = \frac{1}{2}\sin[2\theta(r)]. \tag{3.2}$$

The solution obeying the appropriate boundary condition is[16]

$$\theta_\infty(r) = f(r/\ell), \tag{3.3a}$$

with

$$f(x) = 2\,\arctan(1/x). \tag{3.3b}$$

The length scale ℓ is arbitrary at this point and will be determined later from the requirement $\theta(r=R<\infty)=0$. For $R \gg 1$ it will turn out that $\ell \propto \sqrt{R}$. The skyrmion solution is schematically shown in Fig. 5.

B. Perturbation theory for $R \gg 1$

We now determine the corrections to the zeroth order solution. Let us write $\theta(r)=\theta_\infty(r)+\delta\theta(r)$ and $a(r)=a_\infty(r)+\delta a(r)$ and require $|\delta a(r)| \ll |a_\infty(r)|$ and $|\delta\theta(r)| \ll 1$.[29] An inspection of the ODEs [Eq. (2.17)] shows that, for $r \lesssim O(\ell)$, the corrections can be expanded in a series in powers of $1/\ell$,

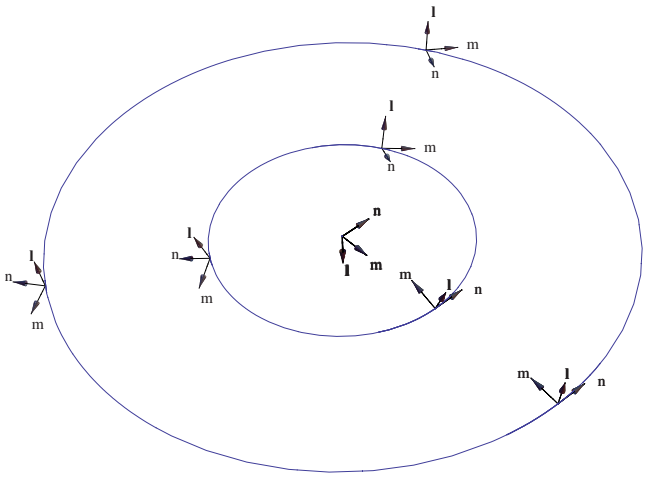

FIG. 5. (Color online) Configurations of the vectors $\hat{\ell}$, $\hat{m}$, and $\hat{n}$ for a skyrmion. Notice that the vector shown in Fig. 2(b) is $\hat{\ell}$.

$$\delta\theta(r) = \frac{1}{\ell^2}g(r/\ell) + \frac{1}{\ell^4}h(r/\ell) + O(1/\ell^6), \tag{3.4a}$$

$$\delta a(r) = \frac{1}{\ell^3}\alpha(r/\ell) + \frac{1}{\ell^5}\beta(r/\ell) + O(1/\ell^7). \tag{3.4b}$$

The functions α and β can be determined by substituting Eq. (3.4b) in Eq. (2.17b), and equating coefficients of powers of $1/\ell$. The resulting equations for α and β are linear *algebraic* equations, not ODEs, because terms involving derivatives of α and β only enter at higher order in $1/\ell$, as one can verify by direct calculation. Hence, the solutions for α and β can be read off at once and are

$$\alpha(x) = \frac{16x}{(1+x^2)^3}, \tag{3.5a}$$

$$\beta(x) = 2\frac{(3x^4-6x^2-1)}{x^2(1+x^2)^3}g(x) - 2\frac{(3x^2-1)}{x(1+x^2)^2}g'(x) + \frac{2}{1+x^2}g''(x) + A(x), \tag{3.5b}$$

where

$$A(x) = \alpha''(x) + \frac{1}{x}\alpha'(x) - \frac{1}{x^2}\alpha(x) = \frac{384x(x^2-1)}{(1+x^2)^5}. \tag{3.5c}$$

Similarly, by comparing coefficients in Eq. (2.17a) we find ODEs for the functions g and h,

$$g''(x) + \frac{1}{x}g'(x) - \frac{1}{x^2}\cos[2f(x)]g(x) = -\frac{2}{x}\sin[f(x)]\alpha(x), \tag{3.6a}$$

$$h''(x) + \frac{1}{x}h'(x) - \frac{1}{x^2}\cos[2f(x)]h(x)$$
$$= -\frac{2}{x}\sin[f(x)]\beta(x) - \frac{1}{x^2}\sin[2f(x)]g^2(x)$$
$$-\frac{2}{x}\cos[f(x)]\alpha(x)g(x), \tag{3.6b}$$

with $f(x)$ from Eq. (3.6b).

The ODE [Eq. (3.6a)] for g can be solved by standard methods (see Appendix B). The physical solution is the one that vanishes for $x \to 0$; it is proportional to x for $x \gg 1$. We find

$$g(x) = -\frac{4}{3}\frac{x[x^2(4+x^2) + 2(1+x^2)\ln(1+x^2)]}{(1+x^2)^2}, \tag{3.7a}$$

the large-x asymptotic behavior of which is

$$g(x \gg 1) = -\frac{4}{3}x - \frac{16}{3}\frac{\ln x}{x} - \frac{8}{3x} + O\left(\frac{\ln x}{x^2}\right). \tag{3.7b}$$

This determines both the function $\beta(x)$ [Eq. (3.5b)] and the inhomogeneity of the ODE [Eq. (3.6b)] for $h(x)$. The latter can again be solved in terms of tabulated functions (see Appendix B) but we will need only the two leading terms for $x \to \infty$. The physical solution is again the one that vanishes for $x \to 0$, and its large-x asymptotic behavior is

$$h(x \gg 1) = -\frac{32}{9}x \ln x + \frac{536}{135}x + O(1/x). \tag{3.8}$$

Finally, we need to fix the length scale ℓ. It is determined by the requirement $\theta(r=R)=0$. We find

$$\ell^2 = \sqrt{\frac{c}{2}}R\left[1 + \frac{\sqrt{2c}}{R}\ln R + \frac{\delta}{R} + O\left(\frac{\ln R}{R^{3/2}}\right)\right], \tag{3.9a}$$

where

$$\delta = \sqrt{2c}\left[\frac{1}{12}(7 - 6d/c^2) - \frac{1}{2}\ln(c/2)\right], \tag{3.9b}$$

and

$$c = 4/3, \tag{3.9c}$$

$$d = 536/135, \tag{3.9d}$$

are the absolute values of the coefficients of the terms proportional to x in the large-x expansions of $g(x)$ and $h(x)$, respectively. We see that, for $R \gg 1$, ℓ is indeed proportional to $\sqrt{R}$, as we had anticipated above. That is, the characteristic skyrmion length scale ℓ is the geometric mean of the London penetration depth λ (recall that we measure all lengths in units of λ) and the skyrmion size R. We now can also check our requirement $\delta\theta \ll 1$: from Eq. (3.4a) we see that for $r \ll \ell$, $\delta\theta(r) \propto 1/R$, while for $r \gg \ell$, $\delta\theta(r)$ is bounded by a term proportional to $1/R^{1/2}$. For R large compared to the penetration depth the condition is thus fulfilled for all r. Similarly, δa is found to be small compared to a_∞ for all r.

C. Energy of a single skyrmion

By using our perturbative solution in Eq. (2.16), we are now in a position to calculate the energy of a single skyrmion to $O(1/R^2)$. It is convenient to first expand the energy in powers of $1/\ell^2$ and then determine the R dependence by using Eq. (3.9).

Let us first consider the supercurrent energy E_c, i.e., the second term in Eq. (2.16). It can be written as

$$E_c/E_0 = \int_0^R drr[\delta a(r)]^2 = \frac{1}{\ell^6}\int_0^R drr[\alpha(r/\ell)]^2 + O(1/\ell^6). \tag{3.10}$$

Using Eq. (3.5a) we find

$$E_c/E_0 = \frac{32}{5}\frac{1}{\ell^4} + O(1/\ell^6). \tag{3.11}$$

Now consider the magnetic energy E_m, which is the third term in Eq. (2.16). It can be written

$$E_m/E_0 = \int_0^R drrb^2(r), \tag{3.12}$$

with

$$b(r) = \frac{1}{r}a_\infty(r) + a'_\infty(r) + \frac{1}{r}\delta a(r) + \delta a'(r), \tag{3.13a}$$

as the magnetic induction in our reduced units. Notice that, in calculating $a_\infty(r)$, $\theta(r)$ in Eq. (3.1) needs to be expanded to first order in $\delta\theta$, as noted earlier. The two leading contributions to b^2 are then

$$b^2(r) = \frac{16}{\ell^4}\frac{1}{(1+x^2)^4} - \frac{8}{\ell^6}\frac{1}{(1+x^2)^2}\left[2\frac{1-x^2}{x(1+x^2)^2}g(x) + \frac{2g'(x)}{1+x^2} + \frac{1}{x}\alpha(x) + \alpha'(x)\right] + O(1/\ell^8), \tag{3.13b}$$

where $x = r/\ell$. Performing the integral yields

$$E_m/E_0 = \frac{8}{3}\frac{1}{\ell^2} - \frac{112}{135}\frac{1}{\ell^4} + O(1/\ell^6). \tag{3.14}$$

Finally, we need to calculate the energy E_s coming from the gradient terms in the first term in Eq. (2.16). The expansion of the two terms in the integrand yields seven integrals that contribute to the desired order; they are listed in Appendix C. The result is

$$E_s/E_0 = 2 + \frac{8}{3}\frac{1}{\ell^2} + \frac{64}{9}\frac{\ln\ell}{\ell^4} + \left(-\frac{1832}{135} - 2c\sqrt{2c}\delta + 4c^2\ln(2/c)\right)\frac{1}{\ell^4} + O(1/\ell^6). \tag{3.15}$$

Adding the three contributions and using Eq. (3.9), we find our final result for the energy of a skyrmion of radius $R \gg 1$,

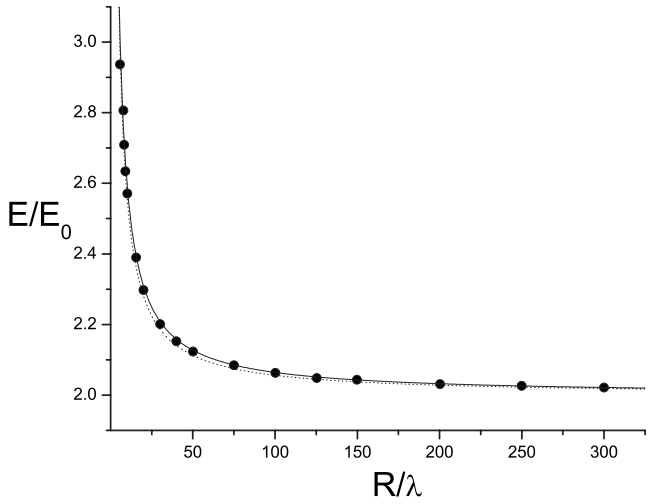

FIG. 6. Numerical data for the energy per skyrmion per unit length (circles) together with the best fit to a pure $1/R$ behavior (dashed line) from Ref. 16, and the perturbative analytic solution given by Eq. (3.16) (solid line). A numerical solution using spectral methods is indistinguishable from the perturbative one.

$$E/E_0 = 2 + \frac{8\sqrt{6}}{3}\frac{1}{R} - \frac{16}{3}\frac{\ln R}{R^2} - \frac{4}{45}[7 + 30\ln(3/2)]\frac{1}{R^2} + O(\ln^2 R/R^3). \quad (3.16)$$

Knigavko *et al.*[16] solved Eq. (2.17) numerically, and thereby numerically determined the energy, which they fit to a $1/R$ dependence. Their results are shown in Fig. 6 together with the analytical result given in Eq. (3.16). The perturbative solution up to $O(\ln R/R^2)$ was first given in Ref. 21. We have also solved the equations numerically using spectral methods to convert the boundary-value problem to a set of algebraic equations for the unknown coefficients in an expansion in Chebyshev polynomials.[30] For the R range shown and on the scale of the figure, the result is indistinguishable from the perturbative one.

IV. OBSERVABLE CONSEQUENCES OF THE SKYRMION ENERGY

Our calculation of the skyrmion energy in Sec. III has been for a cylindrically symmetric skyrmion. The result shows that each skyrmion will try to maximize its radius in order to minimize the energy, which leads to a repulsive interaction between skyrmions whose potential is proportional to $1/R$. Skyrmions are thus expected to form a lattice structure, as do vortices, and they will thus *not* be cylindrically symmetric since the lattice is not. One expects a hexagonal lattice, as in the case of the vortex lattice, and our treatment involves the same approximation as in the numerical work of Ref. 16; namely, approximating the hexagonal unit cell by a circle of the same area. We expect this approximation to recover the correct scaling of the energy, and reproducing the coefficients of that scaling to the same accuracy as radius of the circle of the same area reproduces the distance from the center of a hexagon to the nearest point on its edge, i.e., $\sqrt{2\sqrt{3}/\pi} - 1 \approx 0.05$. We will now proceed to calculate observable consequences of the dependence of the energy on the radius of the unit cell. These include the relation $B(H)$ between the magnetic induction B and the external magnetic field H, the elastic properties of the skyrmion lattice and the resulting phase diagram in the H-T plane, and the μSR signature of the skyrmion lattice.

A. $B(H)$ for a skyrmion lattice

We start by calculating the dependence of the equilibrium lattice constant R on an external magnetic field H. This is done by minimizing the energy per unit volume, which is the energy per unit length per skyrmion [Eq. (3.16)] divided by the area per skyrmion, πR^2, plus a reduction in the energy of $-2\Phi_0 H/4\pi$ due to the external field. The latter is obtained from the last term in Eq. (2.8) by noting that the magnetic flux $\int dxdy(\hat{z}\cdot\boldsymbol{b}) = 2\Phi_0$ for each skyrmion in the lattice. This negative external field contribution must also be divided by πR^2 to give the energy per unit volume. Returning to ordinary units, we thus find a Gibbs free energy per unit volume

$$g(R) = \frac{K}{4\pi^2}\left\{-\frac{\Delta}{R^2} + \frac{4\sqrt{6}\lambda}{3R^3} + O\left[\frac{\lambda^2\ln(R/\lambda)}{R^4}\right]\right\}, \quad (4.1)$$

where $K = \Phi_0^2/2\pi\lambda^2$, and

$$\Delta \equiv 1 - H/H_{c1}, \quad (4.2)$$

with $H_{c1} \equiv K/2\Phi_0$. For $H < H_{c1}$, we have $\Delta > 0$, and the free energy is minimized by $R = \infty$, i.e., the skyrmion density is zero. This is the Meissner phase. For $H > H_{c1}$ the free energy is minimized by

$$R = R_0 = 2\sqrt{6}\lambda/\Delta, \quad (4.3)$$

and there is a nonzero skyrmion density. We see that H_{c1} is indeed the lower critical field. Note that the equilibrium flux lattice constant R_0 diverges as $1/\Delta$, whereas in the case of a vortex lattice it diverges only logarithmically as $\ln(1/\Delta)$.[1] For the averaged magnetic induction $B = 2\Phi_0/\pi R_0^2$, this implies

$$B(H) = \frac{1}{3}H_{c1}\Delta^2. \quad (4.4)$$

For $H \to H_{c1}$ from above, $B(H)$ in the case of a skyrmion lattice thus vanishes with zero slope, whereas in the case of a vortex lattice it vanishes with an infinite slope.[1] This result, with a slightly different prefactor, was first obtained from the aforementioned numerical determination of $E(R)$ in Ref. 16. Note that the only material parameter that appears in this expression for B is H_{c1}.

B. Elastic properties of the skyrmion lattice

Now we turn to the elastic properties of skyrmion lattice. Let the equilibrium position of the ith skyrmion line be described by a two-dimensional lattice vector $\boldsymbol{R}_i = (X_i, Y_i)$, and the actual position by

$$\boldsymbol{r}_i(z) = [X_i + u_x(\boldsymbol{R}_i, z), Y_i + u_y(\boldsymbol{R}_i, z), z], \tag{4.5}$$

where $\boldsymbol{u} = (u_x, u_y)$ is the two-dimensional displacement vector, and we use z as the parameter of the skyrmion line. The strain tensor $u_{\alpha\beta}$ is defined as

$$u_{\alpha\beta}(\boldsymbol{x}) = \frac{1}{2}\left(\frac{\partial u_\alpha}{\partial x_\beta} + \frac{\partial u_\beta}{\partial x_\alpha}\right). \tag{4.6}$$

For a hexagonal lattice of lines parallel to the z axis, the elastic Hamiltonian is[31]

$$H_{\rm el} = \frac{1}{2}\int d\boldsymbol{x}\{2\mu[u_{\alpha\beta}(\boldsymbol{x})u_{\alpha\beta}(\boldsymbol{x})] + \lambda_L[u_{\alpha\alpha}(\boldsymbol{x})]^2 + K_{\rm tilt}|\partial_z \boldsymbol{u}(\boldsymbol{x})|^2\}. \tag{4.7}$$

Here summation over repeated indices is implied. μ, λ_L, and $K_{\rm tilt}$ are the shear, bulk, and tilt moduli, respectively, of the lattice, and we now need to determine these elastic constants.

The combination $\mu+\lambda_L$ can be obtained by considering the energy change in the system upon a dilation of the lattice. Let R change from R_0 to $R_0(1+\epsilon)$, with a dilation factor $\epsilon \ll 1$. Such a dilation corresponds to a displacement field $\boldsymbol{u}(\boldsymbol{x}) = \epsilon \boldsymbol{x}_\perp$, where $\boldsymbol{x}_\perp$ is the projection of $\boldsymbol{x}$ perpendicular to the z axis.[31] The strain tensor is thus $u_{\alpha\beta} = \epsilon\delta_{\alpha\beta}$. Inserting this in the elastic Hamiltonian [Eq. (4.7)] yields the energy per unit volume for the dilation,

$$E_{\rm dil}/V = 2(\mu + \lambda_L)\epsilon^2. \tag{4.8a}$$

This should be compared with the energy as given by Eq. (4.1),

$$E_{\rm dil}/V = g[R_0(1+\epsilon)] - g(R_0) = \frac{1}{2}\left(\frac{\partial^2 g}{\partial R^2}\right)_{R_0}(\epsilon R_0)^2 = \frac{K\Delta^3}{96\pi^2\lambda^2}\epsilon^2. \tag{4.8b}$$

Comparing Eqs. (4.8a) and (4.8b) yields

$$\mu + \lambda_L = K\Delta^3/192\pi^2\lambda^2. \tag{4.9}$$

To obtain μ (or λ_L) separately, we need to consider shear deformations, which change the shape but not the area of the unit cell. Here we will give some elementary arguments that give the correct scaling of μ with Δ (but not the correct prefactors); in Appendix D we present a more technical and thorough treatment. The salient question is the functional form of the skyrmion pair potential $V(r)$ that results in the Gibbs free energy given in Eq. (4.1). $V(r) \propto 1/r$ is *not* the correct answer, the leading R dependence of E in Eq. (3.16), or the second term in Eq. (4.1), notwithstanding, since ℓ constitutes an additional length scale that depends on R. In Appendix D [see Eq. (D5)] we show that

$$V(r) \propto K\lambda R^{\gamma-1}/r^\gamma, \tag{4.10}$$

with $\gamma > 2$ and the proportionality constant a number of $O(1)$. This result allows us to estimate the shear modulus as follows.

If the lattice is subjected to a uniform x-y shear—i.e., a displacement field $\boldsymbol{u}(\boldsymbol{x}) = 2\epsilon y\hat{\boldsymbol{x}}$—for which $u_{xy} = u_{yx} = \epsilon$, and all other components of $u_{\alpha\beta} = 0$, the elastic energy [Eq. (4.7)] predicts an elastic energy per unit volume of

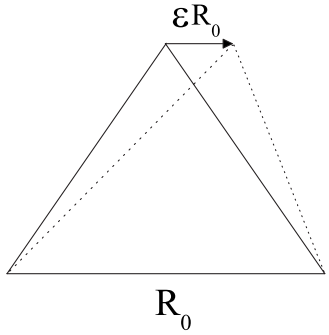

FIG. 7. Shearing of the skyrmion lattice results in a change in the distance between skyrmion centers, and hence in their effective interaction. See the text for additional information.

$$E/V = 2\mu\epsilon^2. \tag{4.11}$$

Such a shear skews each fundamental triangle of the skyrmion lattice by displacing the top (or bottom, for the downward-pointing triangles) to the right (or the left, for downward-pointing triangles) by an amount of order of ϵR_0, where R_0 is the skyrmion lattice spacing found earlier [Eq. (4.3)] (see Fig. 7).

This shortens the length of one bond of the triangle from R_0 to $R_0[1-\sqrt{3}\epsilon/2+9\epsilon^2/8+O(\epsilon^3)]$, and it lengthens to other bond to $R_0[1+\sqrt{3}\epsilon/2+9\epsilon^2/8+O(\epsilon^3)]$. Hence, the linear in ϵ change in the "equivalent potentials" of these two bonds cancels, and the total change $(\Delta E/\text{triangle})$ in the energy per unit length of fundamental triangle, per triangle, is given by:

$$\frac{\Delta E}{\text{triangle}} = \frac{3}{4}[3R_0V'(R_0) + V''(R_0)]\epsilon^2 + O(\epsilon^3). \tag{4.12}$$

With $V(r)$ as given by Eq. (4.10) we find

$$\frac{\Delta E}{\text{triangle}} = \frac{K\lambda}{R_0}\epsilon^2 \times O(1). \tag{4.13}$$

Notice that the prefactor of $O(1)$ is proportional to $\gamma(\gamma-2)$, and hence positive only for $\gamma > 2$, which is ascertained by the arguments given in Appendix D. This is the change in energy per unit cell. To get the energy per unit volume, we must divide by the unit-cell area, which is πR_0^2. Doing so gives

$$\frac{\Delta E}{V} = \frac{K\lambda}{R_0^3}\epsilon^2 \times O(1). \tag{4.14}$$

Comparing this with Eq. (4.11) then determines μ,

$$\mu = \frac{K\lambda}{R_0^3} \times O(1). \tag{4.15}$$

Using Eq. (4.3) for R_0 then leads to our final result for μ,

$$\mu = \frac{K\Delta^3}{\lambda^2} \times O(1). \tag{4.16a}$$

From Eq. (4.9) we see that the bulk modulus or Lamè coefficient is given by the same expression,

$$\lambda_L = \frac{K\Delta^3}{\lambda^2} \times O(1). \tag{4.16b}$$

These elementary considerations yield the homogeneous or local (zero-wave-number) values of the elastic moduli, and they take into account only nearest-neighbor interactions. In Appendix D we show that the scale of the wave-number dependence of μ and λ_L is given by the inverse lattice spacing, $1/R_0$, so taking into account nonlocal effects just changes the prefactors of $O(1)$ in the considerations below. We also go beyond the nearest-neighbor approximation and show that, again, only the numerical values of prefactors are affected by this approximation.

We now turn to the tilt modulus $K_{\rm tilt}$. This can be obtained by considering a uniform tilt of the axes of the skyrmions away from the z axis, i.e., away from the direction of the external magnetic field H, by an angle $\vartheta \ll 1$. For small ϑ, $\vartheta = |\partial \boldsymbol{u}/\partial z|$. Therefore, the tilt energy in Eq. (4.7) is identical with the change in the $\boldsymbol{B}\cdot\boldsymbol{H}$ term in Eq. (2.8). This contribution to the energy is, per unit length and in ordinary units, given by $-\Phi_0 H \cos\theta/2\pi$, and its change due to tilting is $\Phi_0 H(1-\cos\vartheta)/2\pi \approx \Phi_0 H\vartheta^2/4\pi = \Phi_0 H|\partial_z \boldsymbol{u}|^2/4\pi$. Dividing this result by the unit-cell area πR_0^2, using Eq. (4.3) for R_0, and identifying the result with the tilt term in the elastic Hamiltonian [Eq. (4.7)], yields $K_{\rm tilt}$ in the vicinity of H_{c1},

$$K_{\rm tilt} = \frac{1}{12\pi} H_{c1}^2 \Delta^2. \tag{4.17}$$

Again, this is the zero-wave-number value of $K_{\rm tilt}$. In Appendix D we show that taking into account the wave-number dependence of $K_{\rm tilt}$ leads only to quantitative changes in our conclusions.

We now are in a position to calculate the mean-square positional fluctuations $\langle|\boldsymbol{u}(\boldsymbol{x})|^2\rangle$. Taking the Fourier transform of Eq. (4.7), and using the equipartition theorem, yields

$$\langle|\boldsymbol{u}(\boldsymbol{x})|^2\rangle_T = \frac{k_B T}{V} \sum_{\boldsymbol{q}\in \rm BZ} \frac{1}{\mu q_\perp^2 + K_{\rm tilt} q_z^2} \tag{4.18a}$$

for the transverse fluctuations and

$$\langle|\boldsymbol{u}(\boldsymbol{x})|^2\rangle_L = \frac{k_B T}{V} \sum_{\boldsymbol{q}\in \rm BZ} \frac{1}{(2\mu+\lambda_L) q_\perp^2 + K_{\rm tilt} q_z^2} \tag{4.18b}$$

for the longitudinal ones. Here $\boldsymbol{q}_\perp$ and q_z are the projections of the wave vector $\boldsymbol{q}$ orthogonal to and along the z direction, respectively. The Brillouin zone (BZ) of the skyrmion lattice is a hexagon (which we have approximated by a circle) of edge length $O(1)/R_0$ in the plane perpendicular to the z axis, and extends infinitely in the z direction.

Since μ and λ_L are the same apart from a prefactor of $O(1)$ which we have not determined [see Eq. (4.16)], the same is true for the transverse and longitudinal contributions to the fluctuations, and it suffices to consider the former. Performing the integral over q_z yields

$$\langle|\boldsymbol{u}(\boldsymbol{x})|^2\rangle = \langle|\boldsymbol{u}(\boldsymbol{x})|^2\rangle_L + \langle|\boldsymbol{u}(\boldsymbol{x})|^2\rangle_T \propto \langle|\boldsymbol{u}(\boldsymbol{x})|^2\rangle_T = \frac{k_B T}{\sqrt{\mu K_{\rm tilt}}} \int_{\rm BZ} \frac{d^2 q_\perp}{8\pi^2} \frac{1}{q_\perp}. \tag{4.19}$$

The remaining integral over the perpendicular part of the Brillouin zone is proportional to $1/R_0$, and using Eqs. (4.3) we obtain

$$\langle|\boldsymbol{u}(\boldsymbol{x})|^2\rangle = \frac{k_B T}{\lambda H_{c1}^2} \frac{1}{\Delta^{3/2}} \times O(1). \tag{4.20}$$

Using Eq. (4.3) again we see that, near H_{c1}, $\langle|\boldsymbol{u}(\boldsymbol{x})|^2\rangle \propto R_0^{3/2} \ll R_0^2$. That is, in this regime the positional fluctuations are small compared to the lattice constant, which tells us that the lattice will be stable against melting. To elaborate on this, let us consider the Lindemann criterion for melting, which states that the lattice will melt when the ratio $\Gamma_L = \langle|\boldsymbol{u}(\boldsymbol{x})|^2\rangle/R_0^2$ exceeds a critical value $\Gamma_c = O(1)$. In our case,

$$\Gamma_L = \frac{k_B T}{H_{c1}^2 \lambda^{5/2}} \Delta^{1/2} \times O(1). \tag{4.21}$$

As $H \to H_{c1}$, $\Delta \to 0$, and the Lindemann ratio vanishes. Hence, the skyrmion lattice does not melt at any temperature for H close to H_{c1}.

We finally determine the shape of the melting curve $H_m(T)$ near the superconducting transition temperature T_c. Since, in mean-field theory, $H_{c1} \propto (T_c - T)$, and $\lambda \propto 1/\sqrt{T_c - T}$,[1] we find from Eq. (4.21) by putting $\Gamma_L = \text{const} = O(1)$,

$$H_m - H_{c1} \propto (T_c - T)^{5/2}. \tag{4.22}$$

The resulting phase diagram is shown schematically in Fig. 8. Comparing with Fig. 1 we see the qualitative difference between the vortex and skyrmion flux lattices: whereas the vortex lattice always melts near H_{c1}, the skyrmion lattice melts nowhere near H_{c1}. This is a direct consequence of the power-law interaction between skyrmions [Eq. (4.10)], as opposed to the screened Coulomb interaction between vortices, and it agrees with what one would intuitively expect: the power-law interaction means a skyrmion lattice is stiffer than a vortex lattice, and hence harder to melt. We also mention again that we have used the local elastic constants to determine the qualitative phase diagram near H_{c1}. As shown in Appendix D, and mentioned after Eq. (4.16) above, the scale for the wave-number dependence of the elastic constants is given by $1/R_0$, and they therefore show only a mild wave-number dependence within the first Brillouin zone. As a result, the Lindemann criterion with local elastic constants is qualitatively accurate, and quantitatively to within a factor of 2 or so. This is in contrast to the case of a vortex lattice near H_{c2}, where the scale for the wave-number dependence of the elastic constants is given by $1/\lambda$. Yet $1/\lambda \ll \pi/R_0$ so the elastic constants show a large variation for wave numbers within the first Brillouin zone that needs to be taken into account.[5] The technical underpinnings of the qualitative arguments given above are presented in Appendix D.

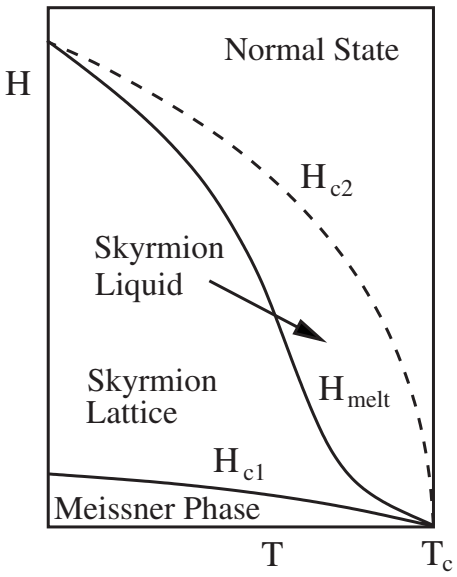

FIG. 8. External field (H) vs temperature (T) phase diagram for skyrmion flux lattices. In contrast to the vortex case (see Fig. 1), there is a direct transition from the skyrmion flux lattice to the Meissner phase. The theory predicts the shape of the melting curve only close to T_c [see Eq. (4.22)]; the rest of the curve is an educated guess.

C. μSR signature of a skyrmion flux lattice

Muon spin rotation (μSR) is a powerful tool which has been extensively applied in study of the vortex state in type-II superconductors.[32,33] A crucial quantity in this type of experiment is the μSR line shape $n(B)$, which is the probability density that a muon experiences a local magnetic induction B and precesses at the Larmor frequency that corresponds to B. It is defined as

$$n(B) \equiv \langle \delta[B(\boldsymbol{x}) - B] \rangle, \tag{4.23}$$

where $B(\boldsymbol{x})$ is the magnitude of the local magnetic induction and $\langle \cdots \rangle$ denotes the spatial average over a flux lattice unit cell.

To predict the μSR line shape for a skyrmion flux lattice near H_{c1}, it is sufficient, for large R_0, to use only the lowest solution for the magnetic induction obtained in Sec. III A. Inserting Eq. (3.3) into Eq. (3.1), we find for the magnetic induction in reduced units

$$b(r) = -\frac{4\ell^2}{(r^2+\ell^2)^2}. \tag{4.24}$$

Restoring physical units then gives

$$B(r) = \frac{H_{c1}\lambda^2}{2}\frac{\ell^2}{(r^2+\ell^2)^2}, \tag{4.25}$$

where we have dropped the minus sign since only the magnitude of B can be detected in μSR measurements.

From Eq. (4.23) we then find, for H near H_{c1}, where our theory is valid,

$$n(B) = \frac{1}{24\sqrt{2}}\left(\frac{H_{c1}\Delta}{B}\right)^{3/2}\frac{1}{H_{c1}} \quad \text{(skyrmions)}. \tag{4.26}$$

Of course, $n(B)$ is only nonzero for those values of B that actually occur inside the unit cell of the skyrmion lattice. From Eq. (4.25), we see that the maximum value of B will occur at the center of the unit cell ($r=0$), which gives

$$|B|_{\max} = |B(r=0)| = \frac{H_{c1}\lambda^2}{2\ell^2} = \frac{H_{c1}\Delta}{8}. \tag{4.27a}$$

The minimum value of B occurs at the edge of the unit cell (i.e., $r=R$), where Eq. (4.25) gives

$$|B|_{\min} = |B(r=R)| = \frac{H_{c1}\lambda^2\ell^2}{2R^4} = \frac{H_{c1}\Delta^3}{288}. \tag{4.27b}$$

In the second equalities in Eq. (4.27) we have used Eqs. (3.9) and (4.3) to express ℓ in terms of R and R in terms of Δ, respectively.

To summarize, the prediction of our cylindrical approximation for $n(B)$ is that the simple power law Eq. (4.26) holds for $B_{\min} < B < B_{\max}$. For $B < B_{\min}$ or $B > B_{\max}$, $n(B)=0$.

Since the above results were derived in the cylindrical approximation, we expect the numerical coefficients in Eq. (4.27) to be off by the approximately 5%, mentioned in the opening paragraph of Sec. IV throughout most of the range $B_{\min} < B < B_{\max}$. When B gets close to $B_{\min}$, however, we expect more radical departures from the cylindrical approximation. This is because contours of constant B near the edge of the hexagonal unit cell will, for B within 5% or so of $B_{\min}$ or so start intersecting the unit-cell boundary, leading to van Hove-type singularities in $n(B)$. Such subtleties cannot be captured within the cylindrical approximation. Note that, however, they only occur over a very small range of B; for the remainder of the large window $B_{\min} < B < B_{\max}$ (which spans three decades even for Δ as big as 0.2), Eq. (4.26) holds, up to the aforementioned 5% numerical error in its overall coefficient.

To compare this result with the corresponding one for a vortex flux lattice, we recall that, in that case, $B(r)$ is given by a modified Bessel function which for distances $r \gg \lambda$ takes the form

$$B(r) \propto \frac{1}{\sqrt{r/\lambda}} e^{-r/\lambda}. \tag{4.28}$$

For small B, we then find from Eq. (4.23)

$$n(B) \propto \frac{\ln(1/B)}{B} \quad \text{(vortices)}. \tag{4.29}$$

We see that the μSR line shape is qualitatively different in the two cases due to the algebraic nature of $B(r)$ in the skyrmion case versus the exponential decay in the vortex case.

V. CONCLUSION

In summary, we have considered properties of a flux lattice formed by the topological excitations commonly referred to as skyrmions rather than by ordinary vortices. For strongly type-II materials in the β phase, skyrmions are more stable than vortices.[16] We have presented an analytical calculation of the energy of a cylindrically symmetric skyrmion of ra-

dius R up to $O(1/R^2)$ in an expansion in powers of $1/R$. This provides excellent agreement with numerical solutions of the skyrmion equations. The interaction between neighboring skyrmion cells falls off only as the inverse lattice constant, in contrast to the exponentially decaying interaction between vortices. As a result, the elastic properties of a skyrmion flux lattice are very different from those of a vortex flux lattice, which leads to qualitatively different melting curves for the two systems. The phase diagram thus provides a smoking gun for the presence of skyrmions. In addition, the μSR line width for skyrmions is qualitatively different from the vortex case.

We finally mention three limitations of our discussion. First, we have restricted ourselves to a discussion of a particular p-wave ground state, namely, the nonunitary state sometimes referred to as the β phase. This state breaks time-reversal symmetry, and the recently reported absence of experimental evidence for the latter in Sr_2RuO_4 (Ref. 34) suggests to also consider other possible p-wave states and their topological excitations, in analogy to the rich phenomenology in helium 3.[11] Second, in a real crystalline material, crystal-field effects will invalidate our isotropic model at very long distances and cause the skyrmion interaction to fall off exponentially. This is the same effect that makes, for instance, the isotropic Heisenberg model of ferromagnetism inapplicable at very long distances and gives the ferromagnetic magnons a small mass. It should be emphasized that this is usually an extremely weak effect that is also material dependent. Once p-wave superconductivity has been firmly established in a particular material, this point needs to be revisited in order to determine the energy scales on which the above analysis is valid. Third, we have worked in a saddle-point approximation and have systematically neglected fluctuations. One might wonder whether taking fluctuations into account would qualitatively alter our results. We note that in conventional bulk superconductors the Ginzburg criterion tells us that fluctuations are unimportant except in an unobservably small temperature regime around the superconducting phase transition. This is a result of the long coherence length in most superconductors. High-T_c superconductors are a different case due to their short coherence length, and fluctuations are important. Analogously, our saddle-point treatment of p-wave superconductors is valid as long as the coherence length is large. In any case, the saddle-point theory presented here provides a basis for the treatment of fluctuation effects should future experiments identify p-wave superconductors with a short coherence length.

ACKNOWLEDGMENTS

We thank Tom Devereaux for suggesting the discussion of μSR as a possible probe for skyrmion lattices and Hartmut Monien for a discussion on defects in helium 3. Part of the work was performed at the Aspen Center for Physics and at the Max Planck Institute for the Physics of Complex Systems in Dresden. This work was supported by the NSF under Grant No. DMR-05-29966.

APPENDIX A: PROPERTIES OF ORTHOGONAL UNIT VECTORS

Let $\hat{\boldsymbol{n}}$ and $\hat{\boldsymbol{m}}$ be orthogonal real unit vectors, and $\hat{\boldsymbol{l}}=\hat{\boldsymbol{n}}\times\hat{\boldsymbol{m}}$. Then the normalization condition $\hat{n}_i\hat{n}_i=\hat{m}_i\hat{m}_i=1$ and the orthogonality condition $\hat{n}_i\hat{m}_i=0$ imply

$$\hat{n}_j\partial_i\hat{n}_j=\hat{m}_j\partial_i\hat{m}_j=0, \tag{A1a}$$

$$\hat{n}_j\partial_i\hat{m}_j=-\hat{m}_j\partial_i\hat{n}_j. \tag{A1b}$$

With these relations it is straightforward to show that

$$\partial_i\hat{n}_j\partial_i\hat{n}_j+\partial_i\hat{m}_j\partial_i\hat{m}_j=2(\hat{n}_j\partial_i\hat{m}_j)(\hat{n}_k\partial_i\hat{m}_k)+\partial_i\hat{l}_j\partial_i\hat{l}_j. \tag{A2}$$

Finally, in regions where $\hat{l}(\boldsymbol{x})$ is differentiable, the Mermin-Ho relation[35] holds,

$$\hat{\boldsymbol{l}}\cdot(\partial_i\hat{\boldsymbol{l}}\times\partial_j\hat{\boldsymbol{l}})=\partial_i\hat{\boldsymbol{n}}\cdot\partial_j\hat{\boldsymbol{m}}-\partial_i\hat{\boldsymbol{m}}\cdot\partial_j\hat{\boldsymbol{n}}. \tag{A3}$$

APPENDIX B: SOLUTIONS OF THE ODES FOR g and h

The functions g and h in Sec. III B both satisfy an ODE of the form [see Eqs. (3.5)]

$$F''(x)+\frac{1}{x}F'(x)-\frac{(x^4-6x^2+1)}{x^2(1+x^2)^2}F(x)=q(x), \tag{B1}$$

with an inhomogeneity q given by the right-hand side of Eq. (3.6a) and (3.6b), respectively. It is easy to check that the corresponding homogeneous equation, obtained from Eq. (B1) by putting $q(x)\equiv 0$, is solved by

$$F_h(x)=x/(1+x^2). \tag{B2}$$

(This is the solution that vanishes as $x\to 0$. The second solution diverges in this limit.) Now write $F(x)=F_h(x)G(x)$, and let $y(x)=G'(x)$. Then y is found to obey the elementary first-order ODE,

$$y'(x)+p(x)y(x)=q(x)/F_h(x), \tag{B3a}$$

with

$$p(x)=[2F_h'(x)+F_h(x)/x]/F_h(x). \tag{B3b}$$

The solution is

$$y(x)=e^{-\int dxp}\left[C_1+\int dxqe^{\int dxp}\right], \tag{B4}$$

with C_1 as an integration constant. A second integration yields $G(x)$, and hence $F(x)$ in terms of two integration constants. The latter can be determined by requiring that for small x the solution coincides with the asymptotic solution that vanishes as $x\to 0$. By using a power-law ansatz for g and h in Eq. (3.6), we find $g(x\to 0)=-8x^3+O(x^4)$, and $h(x\to 0)=256x^3+O(x^4)$, which suffices to fix the integration constants. For $g(x)$ we find the expression given in Eq. (3.7a). For $h(x)$ we obtain

$$h(x) = \frac{1}{[270x(1+x^2)^4]}\{592 + 2x^2[8(-1119 + 90x^2 + 286x^4 + 240x^6 + 30x^8) + 10\,320(1+x^2)^3] + 2296(-1+x^2)(1+x^2)^4 + 4x^2(1+x^2)^3 + 1704\ln x + 32\ln(1+x^2)[-30 + 142x^2 + 276x^4 + 171x^6 + 52x^8 - 15x^{10} - 15(3+x^2)(x+x^3)^2\ln(1+x^2)] - 1920x^2(1+x^2)^3\mathrm{Li}_2(-x^2)\}, \quad \text{(B5)}$$

with Li as the polylogarithm function. The asymptotic behavior for large x is given by Eq. (3.8).

APPENDIX C: CONTRIBUTIONS TO E_s

By expanding the integrand of the first term in Eq. (2.16), we can express the energy E_s to $O(1/R^2)$ in terms of seven integrals,

$$E_s/E_0 = \sum_{i=1}^{7} I_i + O(1/\ell^6), \quad \text{(C1)}$$

with

$$I_1 = 4\int_0^{R/\ell} dx \frac{x}{(1+x^2)^2}, \quad \text{(C2a)}$$

$$I_2 = \frac{2}{\ell^2}\int_0^{R/\ell} dx \frac{1}{1+x^2}\left[\frac{(x^2-1)}{x^2+1}g(x) - xg'(x)\right], \quad \text{(C2b)}$$

$$I_3 = \frac{1}{2\ell^4}\int_0^{R/\ell} dx \left\{x[g'(x)]^2 + \frac{(x^4-6x^2+1)}{x(1+x^2)^2}g^2(x)\right\}, \quad \text{(C2c)}$$

$$I_4 = \frac{2}{\ell^4}\int_0^{R/\ell} dx \frac{1}{1+x^2}\left(\frac{(x^2-1)}{x^2+1}h(x) - xh'(x)\right), \quad \text{(C2d)}$$

$$I_5 = \frac{1}{\ell^6}\int_0^{R/\ell} dx \left(xg'(x)h'(x) + \frac{(x^4-6x^2+1)}{x(1+x^2)^2}g(x)h(x)\right), \quad \text{(C2e)}$$

$$I_6 = -\frac{4}{3\ell^6}\int_0^{R/\ell} dx \frac{(x^2-1)}{(1+x^2)^2}g^3(x), \quad \text{(C2f)}$$

$$I_7 = -\frac{1}{6\ell^8}\int_0^{R/\ell} dx \frac{(x^2-1)^2}{x(1+x^2)^2}g^4(x). \quad \text{(C2g)}$$

Evaluating the integrals to $O(1/\ell^4)$ yields Eq. (3.15).

APPENDIX D: WAVE-NUMBER DEPENDENCE OF THE ELASTIC CONSTANTS

In this appendix we provide the technical details that underlie the arguments given in Sec. IV B. The conclusion is that, for skyrmion lattices near H_{c1}, as opposed to vortex lattices near H_{c2}, the wave-number dependence of the elastic constants is not of qualitative importance for the shape of the phase diagram. For the shear and bulk moduli we reach this conclusion by a qualitative determination of the positional fluctuations of the skyrmion lattice that takes into account nonlocal elastic constants and yields the same result as the calculation in Sec. IV B. For the tilt modulus, length scale considerations show that its dispersion does not change our results for the melting curve either.

1. Shear and bulk moduli

For the shear and bulk moduli we consider, as in Sec. IV B, a set of N parallel skyrmion lines described by a set of set of two-dimensional vectors $\boldsymbol{r}_i$ $(i=1,\ldots,N)$ that are close to, but not necessarily identical with, the equilibrium lattice sites $\boldsymbol{R}_i$. For simplicity, we consider fluctuations in the plane perpendicular to the skyrmion lines only, i.e., we calculate the wave-number dependence of the shear modulus μ and the bulk modulus or Lamé coefficient λ_L. The energy per unit length of this system of skyrmions can be written as

$$E/L_z = 2NE_0 + 2\sum_{\boldsymbol{r}_i \neq \boldsymbol{r}_j} V(\boldsymbol{r}_i - \boldsymbol{r}_j), \quad \text{(D1)}$$

with $2E_0$ as the energy per unit length of a single skyrmion in an infinite system defined after Eq. (2.16), L_z as the length of the system in the direction of the applied magnetic field (which we take to be the z direction), and V as the skyrmion-skyrmion interaction potential. Our goal is now to deduce information about the potential V from the information we have about skyrmions that form a perfect lattice. In the latter case, Eq. (D1) simplifies to

$$E/2NL_z = E_0 + \sum_{\boldsymbol{R}_i \neq \boldsymbol{0}} V(\boldsymbol{R}_i) = E_0\left(1 + \frac{4\sqrt{6}}{3}\frac{\lambda}{R}\right), \quad \text{(D2)}$$

where we have used the leading-order result from Eq. (3.16), with R as the lattice spacing, and we have restored ordinary units. Furthermore, the function $V(\boldsymbol{r})$ must have the same scaling form as any other function of position we have considered so far, namely,

$$V(\boldsymbol{r}) = E_0\left(\frac{\ell}{\lambda}\right)^{\alpha} f(r/\ell), \quad \text{(D3)}$$

with ℓ as the characteristic skyrmion length from Eq. (3.9a). We need to evaluate $V(\boldsymbol{r})$ only for distances $|\boldsymbol{r}| \geq R$, and since $R \gg \ell$ in the region near H_{c1} we are interested in, we need the scaling function f in Eq. (D3) only in the limit $f(x \gg 1)$. Let us anticipate (we will verify this later) that, in this limit, f shows a power-law behavior,

$$f(x \gg 1) = c_\infty x^{-\gamma}, \tag{D4}$$

with c_∞ as a constant of $O(1)$. The scaling law [Eq. (D3)] then implies, in this limit,

$$V(\boldsymbol{r}) = c_\infty E_0 \left(\frac{\ell}{\lambda}\right)^\alpha \left(\frac{\ell}{r}\right)^\gamma = c_\infty E_0 \frac{\ell^{\alpha+\gamma}}{\lambda^\alpha r^\gamma}. \tag{D5}$$

Inserting this into Eq. (D2) yields

$$c_\infty \frac{\ell^{\alpha+\gamma}}{\lambda^\alpha} \sum_{\boldsymbol{R}_i \neq \boldsymbol{0}} \frac{1}{|\boldsymbol{R}_i|^\gamma} = \frac{4\sqrt{6}}{3}\frac{\lambda}{R}. \tag{D6}$$

One constraint imposed by the relation is that the sum on the left-hand side must converge, which implies $\gamma > 2$. Additional information can be gained by scaling the lattice constant out of relation (D6). To this end, we write $\boldsymbol{R}_i = R\boldsymbol{s}_i$, where $\boldsymbol{s}_i$ is a dimensionless vector that runs over the sites of a hexagonal lattice with a unit lattice constant. Using this and Eq. (3.9a), in Eq. (D6) gives

$$c_\infty g(\gamma) \left(\frac{2}{3}\right)^{(\alpha+\gamma)/4} \left(\frac{R}{\lambda}\right)^{(\alpha-\gamma)/2} = \frac{4\sqrt{6}}{3}\frac{\lambda}{R}, \tag{D7a}$$

which confirms our power-law ansatz [Eq. (D4)] and implies

$$\alpha = \gamma - 2. \tag{D7b}$$

Here $g(\gamma) \equiv \Sigma_{s_i \neq \boldsymbol{0}} 1/|\boldsymbol{s}_i|^\gamma = O(1)$ is a number of order unity for all values of γ for which the sum converges. Note that it does not depend on R, λ, or any other material parameter. From Eq. (D5) we thus obtain

$$V(\boldsymbol{r}) = C_\infty E_0 \frac{\ell^{2(\gamma-1)}}{\lambda^{\gamma-2} r^\gamma}, \tag{D8}$$

where C_∞ is another constant of $O(1)$. This, together with expression (3.9a) for ℓ, suffices for a determination of the positional fluctuations, as we will now show.

Consider Eq. (D1) again, and write [see Eq. (4.5)] $\boldsymbol{r}_i = \boldsymbol{R}_i + \boldsymbol{u}(\boldsymbol{R}_i)$, where $\boldsymbol{u}(\boldsymbol{R}_i)$ denotes the displacement field. If we expand to bilinear order in the displacement, we obtain for the (Gibbs free) energy change per unit volume due to the lattice deformation

$$\Delta g = \frac{1}{A} \sum_{\boldsymbol{R}_i \neq \boldsymbol{R}_j} \left.\frac{\partial^2 V}{\partial r_\alpha \partial r_\beta}\right|_{\boldsymbol{r}=\boldsymbol{R}_i-\boldsymbol{R}_j} [u_\alpha(\boldsymbol{R}_i) - u_\alpha(\boldsymbol{R}_j)] \times [u_\beta(\boldsymbol{R}_i) - u_\beta(\boldsymbol{R}_j)], \tag{D9}$$

where $A = L_x L_y = N\pi R^2$ is the cross-sectional area of the system, and a summation over repeated vector indices is implied. Performing a Fourier transform yields, after simple manipulations,

$$\Delta g = \sum_{\boldsymbol{q}_\perp} C_{\alpha\beta}(\boldsymbol{q}_\perp) u_\alpha(\boldsymbol{q}_\perp) u_\beta(-\boldsymbol{q}_\perp), \tag{D10a}$$

where $\mathbf{q}_\perp$ runs over the first Brillouin zone of the lattice and denotes the component perpendicular to the z direction of a three-dimensional wave vector $\mathbf{q}$. Here

$$C_{\alpha\beta}(\boldsymbol{q}_\perp) = \frac{2}{\pi R^2} \sum_{\boldsymbol{R}_i \neq \boldsymbol{0}} \left.\frac{\partial^2 V}{\partial r_\alpha \partial r_\beta}\right|_{\boldsymbol{r}=\boldsymbol{R}_i} [1 - \cos(\boldsymbol{q}_\perp \cdot \boldsymbol{R}_i)]. \tag{D10b}$$

For $\boldsymbol{q}_\perp \to 0$, $C_{\alpha\beta}$ vanishes as $\boldsymbol{q}_\perp^2$. Furthermore, the hexagonal symmetry of the equilibrium lattice implies that $C_{\alpha\beta}$ must have the form

$$C_{\alpha\beta}(\boldsymbol{q}_\perp) = \mu(\boldsymbol{q}_\perp) q_\perp^2 \delta_{\alpha\beta} + [\mu(\boldsymbol{q}_\perp) + \lambda_L(\boldsymbol{q}_\perp)] q_{\perp\alpha} q_{\perp\beta}. \tag{D11a}$$

Here

$$\mu(\boldsymbol{q}_\perp) = \frac{1}{\pi} \sum_{\boldsymbol{R}_i \neq \boldsymbol{0}} P_{\alpha\beta}(\hat{\boldsymbol{q}}_\perp) \left.\frac{\partial^2 V}{\partial r_\alpha \partial r_\beta}\right|_{\boldsymbol{r}=\boldsymbol{R}_i} \frac{1 - \cos(\boldsymbol{q}_\perp \cdot \boldsymbol{R}_i)}{(q_\perp R)^2}, \tag{D11b}$$

and

$$\lambda_L(\boldsymbol{q}_\perp) = -2\mu(\boldsymbol{q}_\perp) + \frac{2}{\pi} \sum_{\boldsymbol{R}_0 \neq \boldsymbol{0}} L_{\alpha\beta}(\hat{\boldsymbol{q}}_\perp) \left.\frac{\partial^2 V}{\partial r_\alpha \partial r_\beta}\right|_{\boldsymbol{r}=\boldsymbol{R}_i} \frac{1 - \cos(\boldsymbol{q}_\perp \cdot \boldsymbol{R}_i)}{(q_\perp R)^2}, \tag{D11c}$$

are the wave vector dependent shear and bulk moduli, respectively. $L_{\alpha\beta}(\hat{\boldsymbol{q}}_\perp) = q_{\perp\alpha} q_{\perp\beta}/q_\perp^2$ and $P_{\alpha\beta}(\hat{\boldsymbol{q}}_\perp) = \delta^\perp_{\alpha\beta} - L^\perp_{\alpha\beta}(\hat{\boldsymbol{q}}_\perp)$ are projection operators that depend only on the unit vector $\hat{\boldsymbol{q}}_\perp = \boldsymbol{q}_\perp/q_\perp$, and $\delta^\perp_{\alpha\beta}$ is the two-dimensional Kronecker symbol.

The preceding considerations are completely general. Now consider the specific potential given in Eq. (D8), which yields

$$\left.\frac{\partial^2 V}{\partial r_\alpha \partial r_\beta}\right|_{\boldsymbol{r}=\boldsymbol{R}_i} = E_0 \frac{\ell^{2(\gamma-1)}}{\lambda^{\gamma-2}} T_{\alpha\beta}(\hat{\boldsymbol{R}}_i)/|\boldsymbol{R}_i|^{\gamma+2}, \tag{D12a}$$

where

$$T_{\alpha\beta}(\hat{\boldsymbol{R}}_i) = C_\infty \gamma [(\gamma+2) R_{0\alpha} R_{0\beta}/\boldsymbol{R}_i^2 - \delta^\perp_{\alpha\beta}] \tag{D12b}$$

is independent of the lattice constant R. Inserting Eq. (D11) into Eqs. (D11b) and (D11c) yields

$$\mu(\boldsymbol{q}_\perp) = E_0 \frac{\lambda}{R^3} f_\mu(q_\perp R, \phi), \tag{D13a}$$

$$B(\boldsymbol{q}_\perp) \equiv 2\mu(\boldsymbol{q}_\perp) + \lambda_L(\boldsymbol{q}_\perp) = E_0 \frac{\lambda}{R^3} f_B(q_\perp R, \phi), \tag{D13b}$$

where

$$f_\mu(q_\perp R, \phi) = \left(\frac{2}{3}\right)^{(\gamma-1)/2} \frac{P_{\alpha\beta}(\hat{\boldsymbol{q}}_\perp)}{(q_\perp R)^2} \frac{1}{\pi} \sum_{\boldsymbol{s}_i \neq \boldsymbol{0}} \frac{T_{\alpha\beta}(\hat{\boldsymbol{s}}_i)}{|\boldsymbol{s}_i|^{\gamma+2}} \times \{1 - \cos[q_\perp R(\boldsymbol{s}_i \cdot \hat{\boldsymbol{q}}_\perp)]\}, \tag{D13c}$$

$$f_B(q_\perp R,\phi)=\left(\frac{2}{3}\right)^{(\gamma-1)/2}\frac{L_{\alpha\beta}(\hat{\boldsymbol{q}}_\perp)q_{\perp\alpha}q_{\perp\beta}R^2}{(q_\perp R)^4}\frac{2}{\pi}\sum_{s_i\neq\mathbf{0}}\frac{T_{\alpha\beta}(\hat{\boldsymbol{s}}_i)}{|\boldsymbol{s}_i|^{\gamma+2}}$$
$$\times\{1-\cos[q_\perp R(\boldsymbol{s}_i\cdot\hat{\boldsymbol{q}}_\perp)]\}. \quad \text{(D13d)}$$

These functions depend on the angle ϕ between $\boldsymbol{q}_\perp$ and, say, the x direction. For $\boldsymbol{q}_\perp=0$, we have $\mu\propto B\propto 1/R^3$, in agreement with Eqs. (4.15). For $\boldsymbol{q}_\perp\neq 0$ these elastic coefficients depend on the modulus of $\boldsymbol{q}_\perp$ only through the combination $q_\perp R$. Therefore, the scale of the $q_\perp$ dependence is given by $1/R$. This is a consequence of the scaling properties of the skyrmion solution, which manifest themselves in Eq. (D3). Moreover it means that the wave-number dependence of μ and λ_L is not important for determining the qualitative shape of the phase diagram near H_{c1}.

2. Tilt modulus

As mentioned in Sec. IV B, the tilt energy is given by the magnetic energy contribution in Eq. (2.8). It can be calculated by a generalization of the method used in Appendix D 1. This is more involved than the calculation of μ and λ_L since the dependence of the magnetic induction on the displacement field $\boldsymbol{u}$ is complicated. However, its qualitative behavior can be deduced by the following simple arguments. The length scale for the decay of the magnetic induction around a skyrmion line is given by ℓ [see Eq. (4.25)]. Therefore, the scale of the q_z dependence of $K_{\rm tilt}$ is given by $1/\ell$. (Notice that there is no periodicity in the z direction, and hence the Brillouin zone extends to infinity in the q_z direction. For a vortex lattice, the corresponding scale is $1/\lambda$.) From Eqs. (4.18a) and (4.18b) we see that the dominant contribution to the integrals that determine the mean-square positional fluctuations comes from q_z on the order of $\sqrt{\mu/K_{\rm tilt}}q_\perp<\sqrt{\mu/K_{\rm tilt}}/R$. Now, $\sqrt{\mu/K_{\rm tilt}}\propto\Delta^{1/2}$ [see Eqs. (4.16) and (4.17)], which vanishes as $H\to H_{c1}$. Therefore, only values of q_z up to $q_z^{\rm max}\equiv\Delta^{1/2}/R\ll 1/R\ll 1/\ell$ are relevant for the elastic properties, and the wave-number dependence of $K_{\rm tilt}$, which becomes appreciable only for $q_z>1/\ell$, is inconsequential.

These results corroborate the considerations in Sec. IV B, which allowed us to use local elastic constants for the qualitative determination of the phase diagram. It is easily confirmed that an explicit calculation of the positional fluctuations, using expression (D13) for the wave vector dependent elastic coefficients μ and λ_L, and including the tilt modulus, recovers Eq. (4.20).

[1] M. Tinkham, *Introduction to Superconductivity* (McGraw-Hill, New York, 1975).
[2] B. A. Huberman and S. Doniach, Phys. Rev. Lett. **43**, 950 (1979).
[3] D. S. Fisher, Phys. Rev. B **22**, 1190 (1980).
[4] D. R. Nelson and H. S. Seung, Phys. Rev. B **39**, 9153 (1989).
[5] E. H. Brandt, Phys. Rev. Lett. **63**, 1106 (1989).
[6] P. L. Gammel, L. F. Schneemeyer, J. V. Waszczak, and D. J. Bishop, Phys. Rev. Lett. **61**, 1666 (1988).
[7] H. Safar, P. L. Gammel, D. A. Huse, D. J. Bishop, J. P. Rice, and D. M. Ginsberg, Phys. Rev. Lett. **69**, 824 (1992).
[8] T. H. R. Skyrme, Proc. R. Soc. London, Ser. A **260**, 127 (1961).
[9] Defects of this general type are known under various names in different contexts, and the action for the defects studied here differs from the one considered by Skyrme. We follow a recent trend to refer to all defects of this type as skyrmions.
[10] P. W. Anderson and G. Toulouse, Phys. Rev. Lett. **38**, 508 (1977).
[11] M. M. Salomaa and G. E. Volovik, Rev. Mod. Phys. **59**, 533 (1987).
[12] D. C. Wright and N. D. Mermin, Rev. Mod. Phys. **61**, 385 (1989).
[13] S. L. Sondhi, A. Karlhede, S. A. Kivelson, and E. H. Rezayi, Phys. Rev. B **47**, 16419 (1993).
[14] C. Timm, S. M. Girvin, and H. A. Fertig, Phys. Rev. B **58**, 10634 (1998), and references therein.
[15] U. Rößler, A. Bogdanov, and C. Pfleiderer, Nature (London) **442**, 797 (2006).
[16] A. Knigavko, B. Rosenstein, and Y. F. Chen, Phys. Rev. B **60**, 550 (1999).
[17] K. D. Nelson, Z. Q. Mao, Y. M. Maeno, and Y. Liu, Science **306**, 1151 (2004).
[18] M. Rice, Science **306**, 1142 (2004).
[19] The precise nature of the order parameter in Sr_2RuO_4 is still being debated (see Ref. 34).
[20] Reference 16 focused on UPt_3, which was the leading candidate for a p-wave superconductor at the time but is now believed to have f-wave symmetry.
[21] Q. Li, J. Toner, and D. Belitz, Phys. Rev. Lett. **98**, 187002 (2007).
[22] The complete order parameter in a p-wave superconductor, or in ^{3}He, also contains an orbital sector (see Ref. 23). For our present purposes the orbital sector is of no importance, and we consider the spin sector only.
[23] D. Vollhardt and P. Wölfle, *The Superfluid Phases of Helium 3* (Taylor & Francis, London, 1990).
[24] See the discussion in Ref. 16, and references therein.
[25] J. Zinn-Justin, *Quantum Field Theory and Critical Phenomena* (Oxford University Press, Oxford, 1996).
[26] More generally, ϕ is an element of the circle or one sphere S_1, and hence $\oint_C d\ell\cdot\nabla\phi(\boldsymbol{x})=2\pi n$, with n as an integer. n is a topological invariant that characterizes the singularity (known as a vortex), and the number of flux quanta that penetrate the vortex is $N=|n|$. The vortex with $n=1$ has the lowest energy within this family of solutions (apart from the trivial "nonvortex" with $n=0$).
[27] R. Rajaraman, *Solitons and Instantons* (North-Holland, Amsterdam, 1982).
[28] More generally, $\int dxdy\epsilon_{ij}\hat{\boldsymbol{l}}\cdot(\partial_i\hat{\boldsymbol{l}}\times\partial_j\hat{\boldsymbol{l}})=8\pi Q$, with Q as an integer. Q is a topological invariant that characterizes the defect (known as a skyrmion), and the number of flux quanta that penetrate the skyrmion is $N=2Q$ (Ref. 16). The skyrmion with $Q=1$ has the lowest energy within this family of solutions.

[29] We emphasize that we do *not* require $|\delta\theta(r)| \ll |\theta_\infty(r)|$, as this requirement is neither necessary nor desirable. Rather, we expand, for instance, $\sin(\theta_\infty+\delta\theta)=\sin\theta_\infty\cos\delta\theta+\cos\theta_\infty\sin\delta\theta=\cos\theta_\infty\,\delta\theta+O(\delta\theta^2)$, which is valid for *all* $\delta\theta \ll 1$, *not* just for those that satisfy $|\delta\theta(r)| \ll |\theta_\infty(r)|$.

[30] J. P. Boyd, *Chebyshev and Fourier Spectral Methods* (Springer, Berlin, 1989).

[31] L. D. Landau and E. M. Lifshitz, *Theory of Elasticity* (Pergamon, Oxford, 1986).

[32] J. E. Sonier, J. H. Brewer, and R. F. Kiefl, Rev. Mod. Phys. **72**, 769 (2000).

[33] A. Schenck, *Muon Spin Rotation: Principles and Applications in Solid State Physics* (Adam Hilger, Bristol, 1986).

[34] P. G. Björnsson, Y. Maeno, M. E. Huber, and K. A. Moler, Phys. Rev. B **72**, 012504 (2005).

[35] N. D. Mermin and T.-L. Ho, Phys. Rev. Lett. **36**, 594 (1976).